

RESEARCH

Open Access



Delta radiomics analysis of Magnetic Resonance guided radiotherapy imaging data can enable treatment response prediction in pancreatic cancer

M. R. Tomaszewski^{1,5}, K. Latifi², E. Boyer³, R. F. Palm³, I. El Naqa⁴, E. G. Moros², S. E. Hoffe³, S. A. Rosenberg³, J. M. Frakes³ and R. J. Gillies^{1*} 

Abstract

Background: Magnetic Resonance Image guided Stereotactic body radiotherapy (MRgRT) is an emerging technology that is increasingly used in treatment of visceral cancers, such as pancreatic adenocarcinoma (PDAC). Given the variable response rates and short progression times of PDAC, there is an unmet clinical need for a method to assess early RT response that may allow better prescription personalization. We hypothesize that quantitative image feature analysis (radiomics) of the longitudinal MR scans acquired before and during MRgRT may be used to extract information related to early treatment response.

Methods: Histogram and texture radiomic features ($n = 73$) were extracted from the Gross Tumor Volume (GTV) in 0.35T MRgRT scans of 26 locally advanced and borderline resectable PDAC patients treated with 50 Gy RT in 5 fractions. Feature ratios between first (F1) and last (F5) fraction scan were correlated with progression free survival (PFS). Feature stability was assessed through region of interest (ROI) perturbation.

Results: Linear normalization of image intensity to median kidney value showed improved reproducibility of feature quantification. Histogram skewness change during treatment showed significant association with PFS ($p = 0.005$, HR = 2.75), offering a potential predictive biomarker of RT response. Stability analyses revealed a wide distribution of feature sensitivities to ROI delineation and was able to identify features that were robust to variability in contouring.

Conclusions: This study presents a proof-of-concept for the use of quantitative image analysis in MRgRT for treatment response prediction and providing an analysis pipeline that can be utilized in future MRgRT radiomic studies.

Introduction

Pancreatic cancer is a deadly disease with survival statistics remaining poor despite intensive research. Locally advanced Pancreatic Ductal Adenocarcinoma (PDAC) has a dismal 5-year survival rate of around 9% [1], with approximately 1/3 of patients expected to die of local

progression [2]. Evaluating therapeutic response of local disease as early as possible is therefore crucial, as maximization of the therapeutic impact to the primary site is critical. For locally advanced patients, evidence has been accumulating that hypofractionated radiotherapy, i.e. stereotactic body radiotherapy (SBRT), can improve both local control and overall survival for these patients [3]. However, it remains a significant challenge to deliver high dose SBRT to pancreatic tumors given their motion and their close proximity to normal structures, such as bowel, that are sources of dose-limiting toxicity [4]. MRI

*Correspondence: Robert.gillies@moffitt.org

¹ Cancer Physiology Department, H. Lee Moffitt Cancer Center and Research Institute, 12902 USF Magnolia Dr, Tampa, FL 33612, USA
Full list of author information is available at the end of the article



© The Author(s) 2021. **Open Access** This article is licensed under a Creative Commons Attribution 4.0 International License, which permits use, sharing, adaptation, distribution and reproduction in any medium or format, as long as you give appropriate credit to the original author(s) and the source, provide a link to the Creative Commons licence, and indicate if changes were made. The images or other third party material in this article are included in the article's Creative Commons licence, unless indicated otherwise in a credit line to the material. If material is not included in the article's Creative Commons licence and your intended use is not permitted by statutory regulation or exceeds the permitted use, you will need to obtain permission directly from the copyright holder. To view a copy of this licence, visit <http://creativecommons.org/licenses/by/4.0/>. The Creative Commons Public Domain Dedication waiver (<http://creativecommons.org/publicdomain/zero/1.0/>) applies to the data made available in this article, unless otherwise stated in a credit line to the data.

guided radiotherapy (MRgRT) is a newer form of radiotherapy that allows for real-time adaptive treatment, tracking of tumor/normal organs, and allows dose escalation to improve the therapeutic window [5].

The excellent soft tissue contrast of MR methods compared to CT provides an opportunity for a dramatic increase in the role of MR in radiotherapy response detection. Through real time imaging, MRgRT technology supplies a dynamic imaging record of tumor changes with every radiation treatment. This information has been used purely for improved planning (better tissue segmentation) and patient setup for radiation delivery. We hypothesize that the wealth of image data provided by MRgRT could also be used to provide a quantitative assessment of intermediate responses and direct the subsequent treatment fractions accordingly. Understanding the patterns of response through automated analysis of imaging data will enable closer monitoring of the tumor changes after irradiation, informing clinical decisions. This is particularly relevant in the setting of those tumors that significantly involve the adjacent vasculature such as those patients with locally advanced pancreatic cancer (LAPC); if enough regression occurs, these tumors may become resectable with negative margins (R0 resection). Decision making at the 4–6 week time point post treatment involves multidisciplinary review which is often complicated by the post MRgRT soft tissue edema. Although the decision to proceed with resection is highly subjective as no consensus guidelines exist [6], some institutions have developed tools to improve prediction of resectability, including data showing that 20% of LAPC patients ultimately could be resected with an improved median overall survival [7]. Automated analysis of the imaging data during treatment could increase the reliability of predicting SBRT success and impact the decision to proceed with resection. PDAC patients may benefit particularly from the advances in MR-based therapy response assessment given their high risk of failure, especially in the unresectable cases.

The emerging field of machine learning in image analytics, or “radiomics”, can provide powerful tools to enable such analysis of the dense MRgRT data. Employing automated high-throughput image feature extraction methods to quantify subtle patterns in the daily images, radiomic analyses [8] have shown great promise for disease prognosis or prediction of treatment response, including radiotherapy [9]. In early proof-of-concept MRgRT radiomic studies, Boldrini et al. [10] considered changes in extracted features using ratios pre- to post-treatment in 16 rectal cancer patients treated on a 0.35T MRgRT system showing promise for response correlation, later they followed up with another study in pancreatic cancer [11]. Simpson et al. [12] looked at static,

absolute values of radiomic features derived from 0.35T MRgRT scans for response prediction in 20 pancreatic cancer patients. With the increasing interest and promise in the field, there is an unmet need for establishing a robust MRgRT image quantification framework to extract the informational content of the imaging data and ensure reproducibility and reliability of extracted features.

Unlike Computed Tomography or Positron Emission Tomography, where pixel/voxel values are related to physical and/or functional properties of the object, absolute MRI signal intensities have no inherent biophysical meaning thereby complicating their radiomic analysis. Image pre-processing and normalization are usually required for efficient quantification of MR signal intensities [13]. Development of an appropriate normalization framework is therefore crucial also for quantitative analysis of MRgRT image data, yet has not been discussed before specifically in the context of this technology. Therefore, in this study an image processing and normalization framework is developed, and feature robustness assessed, with the aim of simplifying and improving the robustness of future MRgRT radiomics analyses.

The short history of MRgRT in routine clinical use limits the availability of patient data, affecting the study design and statistical approaches used in this work. Multivariate, machine learning radiomic analyses cannot confidently be applied in such studies highlighting the importance of feature stability and validation to ensure reproducibility and minimize overfitting [14]. The work described herein is focused on quantification and univariate analysis of changes in standardized [15] radiomic (histogram and texture) image features during treatment.

In this study, we present a robust radiomic framework for quantification of image changes during radiotherapy in pancreatic adenocarcinoma, demonstrating the feasibility of the approach by successful prediction of disease progression in a cohort of 26 borderline/locally advanced PDAC patients who did not undergo surgery after SBRT.

Methods

Data collection

The Institutional Review Board at the University of South Florida approved (IRB #20383) and waived the informed consent requirement for retrospective analysis in this study.

Imaging and follow-up data were compiled from a total of $n = 26$ patients treated with 5 fractions of SBRT on the MRidian (ViewRay Inc., Cleveland, OH) magnetic resonance guided radiotherapy system (also known as a MRI-Linac system) at the Moffitt Cancer Center and that did not undergo resection. The patients were treated to a median dose of 50 Gy to Gross Tumor Volume (GTV).

Progression Free Survival (PFS) was quantified time from MRgRT to latest follow-up or a (local or distant) progression event. Local progression was assessed via RECIST 1.1 using largest tumor diameter in CT scans first obtained approximately 1 month after RT and then every 3 months for one year. An increase of 20% or more represented progressive disease, and a decrease of 30% or more represented partial response. Stable disease was defined as any change between a 20% increase and a 30% decrease. Distant progression was determined by US guided biopsy confirming metastatic disease (most often to the liver), pathology confirmed nodules discovered during exploratory laparotomy (once in liver, once in peritoneum), or by enlarged nodules outside the pancreas on imaging (two instances). Patient demographics are detailed in Table 1.

Each patient received 6 MRI scans with the same protocol, first at simulation (SIM), approximately 14–21 days before the treatment start, and then immediately prior to delivery of each of the 5 radiation fractions (F1–F5). Images were acquired on the MRIdian 0.35T MRI-Linac system using a balanced steady state free precession pulse sequence [16] using the following parameters: TR/TE = 3.33/1.43 ms, flip angle = 60 deg, 310 × 360 points, 144 slices, voxel size 1.5 × 1.5 × 3 mm. Gross Tumor Volume (GTV) was segmented by the radiation oncologist in the SIM scan, and the scans F1–F5 were subsequently

overlaid and co-registered online to the SIM scan. Local manual rigid registration in 3 dimensions was performed in MRIdian treatment console software, directly prior to delivery of each radiation fraction to ensure the GTV is aligned to its position in the SIM scan. This rigid registration was applied to the GTV contour to propagate it from SIM to F1–F5 scans. Processing was performed in the Mirada software (Mirada RTx 1.8, Oxford, UK) by a qualified medical physicist.

Image analysis and feature extraction

All images and Gross Tumor Volume (GTV) regions of interest (ROI) as segmented by the radiation oncologist (JF and SH) were saved in DICOM format and analyzed in MATLAB 2018b (MathWorks Inc., city, state) using custom written code. No spatial interpolation of the images was performed as uniform voxel sizes were used for all scans and patients, and number of intensity bins for texture and histogram feature quantification was fixed at 64.

Prior to image feature quantification, normalization was performed by dividing each image by the corresponding median signal value in the kidney, as practiced in MR radiomics [17] to account for technical intensity variation between imaging sessions. A Kidney ROI was drawn manually for each patient and in each scan in 3 equally spaced slices through the right kidney, as shown in Additional file 1: Fig. S1. Right kidney was chosen as an organ that can be reproducibly delineated in all the scans with no observed image artefacts sometimes seen in superficial areas or towards the peripheral slices. The analysis and rationale behind choosing this normalization approach is described in detail in the Results section. ROIs of the patients' whole abdomen cross-section were automatically generated through image thresholding in 10 slices around the middle of GTV ROI but excluding the GTV. The change in median signal in the abdomen between the simulation and first fraction scans were compared to corresponding changes in the GTV, to quantify the contribution of systemic, technical changes in image intensity to GTV signal.

To avoid overfitting, given the small number of patients, feature extraction was initially confined to histogram features [18] (see Table 2 for feature list) extracted from the GTV to describe the tumor image characteristics. The ratio of each feature between last and first fraction (F5/F1) was quantified as a measure of imaging change after radiation (delta radiomics), and this metric was then analyzed.

In the second part of analysis, N = 62 texture radiomic features were also extracted in 3D from the GTV, and delta radiomics ratios F5/F1 calculated. These features included: Grey Level Co-occurrence Matrix, Grey Level

Table 1 Patient information

Age (years)	66 (60–72)
Sex	
Female	12 (46%)
Male	14 (54%)
Histology	
Adenocarcinoma	26 (100%)
Tumor location	
Head	21 (81%)
Body	4 (15%)
Tail	1 (4%)
Resectability status (at diagnosis)	
Borderline resectable	11 (42%)
Locally advanced	15 (58%)
Induction chemotherapy	
FOLFRINOX	16 (62%)
Gem/Abraxane	6 (23%)
FOLFRINOX and Gem/Abraxane	4 (15%)
Time to progression (days)	120 (60–180)
Follow-up (days)	200 (111–289)

Number quoted is the number of patients in each category for categorical variables, and median value for numerical variables, while the number in brackets signifies percentage of all patients in the category and 25th to 75th percentile range respectively. Follow-up time is quoted for patients who did not progress as time to censoring

Table 2 Feature quantification

Feature class	Feature Name	p value of PFS association	CCC
Histogram features	Mean	0.798 (1.00)	0.998
	Standard_Deviation	0.964 (1.00)	0.991
	Skewness	0.005 (0.038)	0.972
	Kurtosis	0.875 (1.00)	0.979
	Median	0.846 (1.00)	0.998
	Minimum_grey_level	0.941 (1.00)	0.937
	10th_percentile	0.908 (1.00)	0.999
	90th_percentile	0.73 (1.00)	0.994
	Maximum_grey_level	0.916 (1.00)	0.995
	Interquartile_range	0.576 (1.00)	0.989
Statistical_Range	0.748 (1.00)	0.989	
Texture features	avgCooccurrence_Joint_MAX	0.335 (1.00)	0.917
	avgCooccurrence_Joint_Average	0.702 (1.00)	0.823
	avgCooccurrence_Joint_variance	0.282 (1.00)	0.854
	avgCooccurrence_Joint_entropy	0.414 (1.00)	0.953
	avgCooccurrence_Difference_average	0.701 (1.00)	0.969
	avgCooccurrence_Difference_variance	0.984 (1.00)	0.961
	avgCooccurrence_Difference_entropy	0.62 (1.00)	0.964
	avgCooccurrence_Sum_average	0.702 (1.00)	0.823
	avgCooccurrence_Sum_variance	0.355 (1.00)	0.890
	avgCooccurrence_Sum_entropy	0.314 (1.00)	0.928
	avgCooccurrence_Angular_second_moment	0.452 (1.00)	0.965
	avgCooccurrence_Contrast	0.884 (1.00)	0.967
	avgCooccurrence_Dissimilarity	0.701 (1.00)	0.969
	avgCooccurrence_Inverse_difference	0.623 (1.00)	0.973
	avgCooccurrence_Inverse_difference_normalized	0.53 (1.00)	0.970
	avgCooccurrence_Inverse_difference_moment	0.604 (1.00)	0.974
	avgCooccurrence_Inverse_difference_moment_normalized	0.525 (1.00)	0.968
	avgCooccurrence_Inverse_variance	0.265 (1.00)	0.968
	avgCooccurrence_Correlation	0.649 (1.00)	0.979
	avgCooccurrence_Autocorrelation	0.61 (1.00)	0.835
	avgCooccurrence_Cluster_tendency	0.355 (1.00)	0.890
	avgCooccurrence_Cluster_shade	0.049 (1.00)	0.920
	avgCooccurrence_Cluster_prominence	0.756 (1.00)	0.855
	avgCooccurrence_First_measure_of_information_correlation	0.954 (1.00)	0.986
	avgCooccurrence_Second_measure_of_information_correlation	0.962 (1.00)	0.983
	avg_3D_Short_runs_emphasis.	0.666 (1.00)	0.980
	avg_3D_Long_runs_emphasis.	0.747 (1.00)	0.980
	avg_3D_Low_grey_level_run_emphasis.	0.579 (1.00)	0.661
	avg_3D_High_grey_level_run_emphasis.	0.788 (1.00)	0.826
	avg_3D_Short_run_low_grey_level_emphasis.	0.553 (1.00)	0.667
	avg_3D_Short_run_high_grey_level_emphasis.	0.815 (1.00)	0.830
	avg_3D_Long_run_low_grey_level_emphasis.	0.69 (1.00)	0.638
	avg_3D_Long_run_high_grey_level_emphasis.	0.7 (1.00)	0.818
	avg_3D_Grey_level_non_uniformity.	0.533 (1.00)	0.999
	avg_3D_Grey_level_non_uniformity_normalised.	0.545 (1.00)	0.949
	avg_3D_Run_length_non_uniformity.	0.961 (1.00)	1.000
	avg_3D_Run_length_non_uniformity_normalised.	0.658 (1.00)	0.980
	avg_3D_Run_percentage.	0.703 (1.00)	0.981
	avg_3D_Grey_level_variance.	0.619 (1.00)	0.827
	avg_3D_Run_length_variance.	0.896 (1.00)	0.979
	avg_3D_Run_entropy.	0.411 (1.00)	0.904
	GLSZM_Small_zone_emphasis	0.351 (1.00)	0.928
	GLSZM_Large_zone_emphasis	0.9 (1.00)	0.956
	GLSZM_Low_grey_level_zone_emphasis	0.361 (1.00)	0.742
	GLSZM_High_grey_level_zone_emphasis	0.978 (1.00)	0.812
	GLSZM_Small_zone_low_grey_level_emphasis	0.323 (1.00)	0.793
	GLSZM_Small_zone_high_grey_level_emphasis	0.619 (1.00)	0.830
	GLSZM_Large_zone_low_grey_level_emphasis	0.564 (1.00)	0.984
	GLSZM_Large_zone_high_grey_level_emphasis	0.78 (1.00)	0.920
	GLSZM_Grey_level_non_uniformity	0.599 (1.00)	0.999
GLSZM_Grey_level_non_uniformity_normalised	0.912 (1.00)	0.825	
GLSZM_Zone_size_non_uniformity	0.451 (1.00)	0.998	
GLSZM_Zone_size_non_uniformity_normalised	0.35 (1.00)	0.924	
GLSZM_Zone_percentage	0.576 (1.00)	0.975	
GLSZM_Grey_level_variance	0.724 (1.00)	0.803	
GLSZM_Zone_size_variance	0.756 (1.00)	0.953	
GLSZM_Zone_size_entropy	0.586 (1.00)	0.968	
NGTDM_Coarseness	0.984 (1.00)	0.999	
NGTDM_Contrast	0.597 (1.00)	0.919	
NGTDM_Busyness	0.835 (1.00)	0.998	
NGTDM_Complexity	0.732 (1.00)	0.921	
NGTDM_Strength	0.559 (1.00)	0.988	

Table 2 (continued)

Divided by histogram (green) and texture (blue), names of all quantified features (second column), corresponding p value of their association with Progression Free survival (column 3) pre and post (in brackets) multiplicity correction, and the Concordance Correlation Coefficient (CCC) values describing the spatial stability of each feature. P values pre-multiplicity correction are quoted to show the heterogeneity and dynamic range of associations

Run-Length Matrix, Grey Level Size Zone Matrix and Neighboring Gray Tone Difference Matrix features. The extraction protocol was consistent with the Image Biomarker Standardization Initiative [15] to ensure reproducibility of quantification.

Spatial stability of the features was tested by comparing the feature values in the SIM scan in ROIs created by radial erosion or expansion of the GTV by 1.5 mm in each slice, to simulate possible slight differences in GTV segmentation, and identify the least stable features to be avoided in further MRgRT radiomic analysis. Lin's Concordance Correlation Coefficient (CCC) [19], commonly used for agreement quantification was then used to describe the robustness of the features to these small ROI changes.

Statistical analysis

Comparison between imaging changes and progression free survival was performed in the $n=26$ unresected patients. Sixteen progression events were observed, with median time to progression after radiotherapy of 4 months. Locally, a great majority of patients exhibited stable disease by RECIST, with 3 showing progressive disease, and 1 showing a partial response at latest follow-up CT scan.

The statistical analysis was performed using RStudio 1.2.5033 (RStudio Inc, MA, USA) interpreter. Univariate Cox proportional hazard regression model (*coxph* function, *survival* package in R) was used to assess the association between PFS and each feature ratio, separately in histogram and texture features, with Bonferroni-Holm correction applied for multiple comparisons. For features showing significant ($p < 0.05$) association, a conditional inference tree (*ctree* function, *partykit* package) was used to identify the high and low progression risk groups and quantify the optimal feature ratio threshold. The same approach was repeated for texture features.

Results

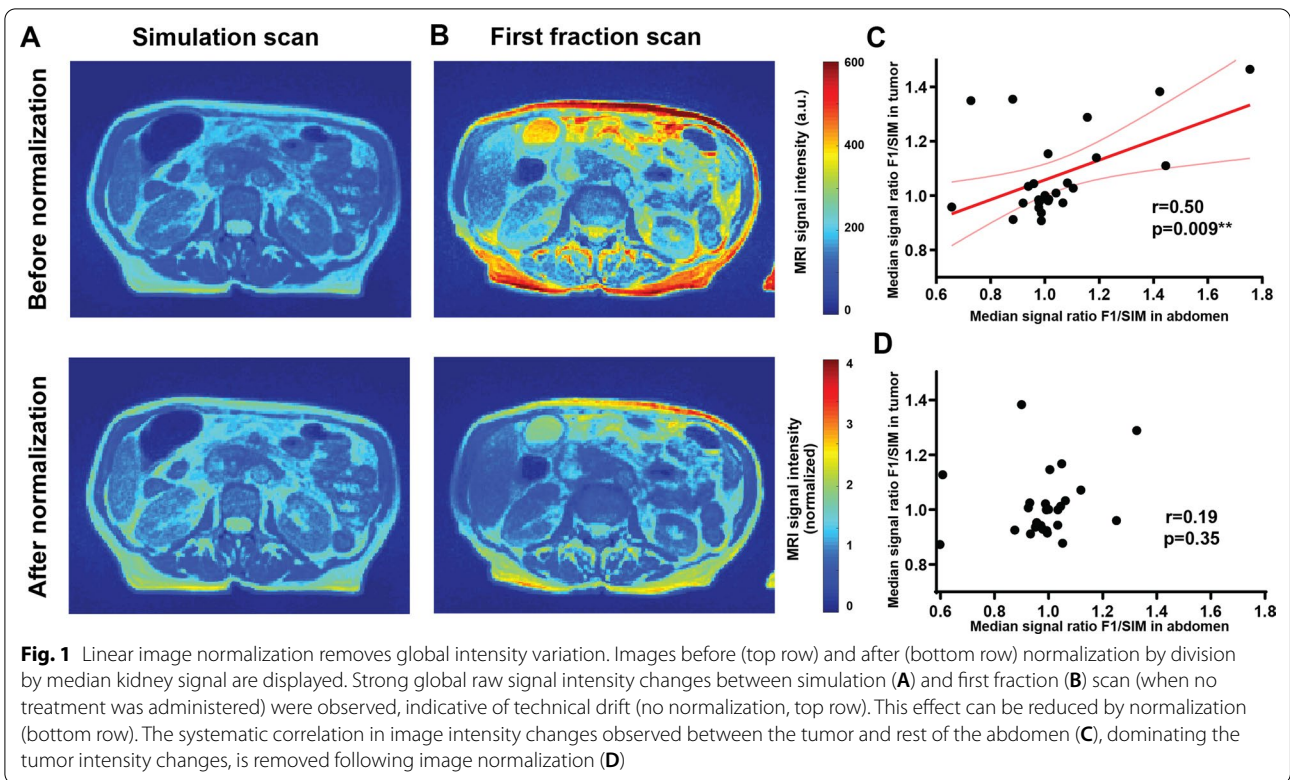
Associations between the patient characteristics and progression-free survival were explored. Patients treated with Gem/Abraxane induction therapy showed significantly worse outcome ($p=0.005$, HR=9.45 (2.37–37.8) and HR=4.63 (1.13–18.9) for Gem/Abraxane only and Gem/Abraxane after FOLFIRINOX, vs. FOLFIRINOX only). This is expected, as Gem/Abraxane tends to be prescribed at our institution to patients in worse overall condition who are less likely to tolerate FOLFIRINOX

treatment. Resectability status at diagnosis showed no association with survival ($p=0.99$).

Streamlined MATLAB code was written to enable integrated readout of the image and segmentation data and metadata, co-registration of the ROIs, normalization and quantification of image features in one pipeline for multiple patients at a time. This code, available at https://github.com/mrtomasz91/MRgRT_PDAC can be easily adapted and reused for further MRgRT image quantification studies.

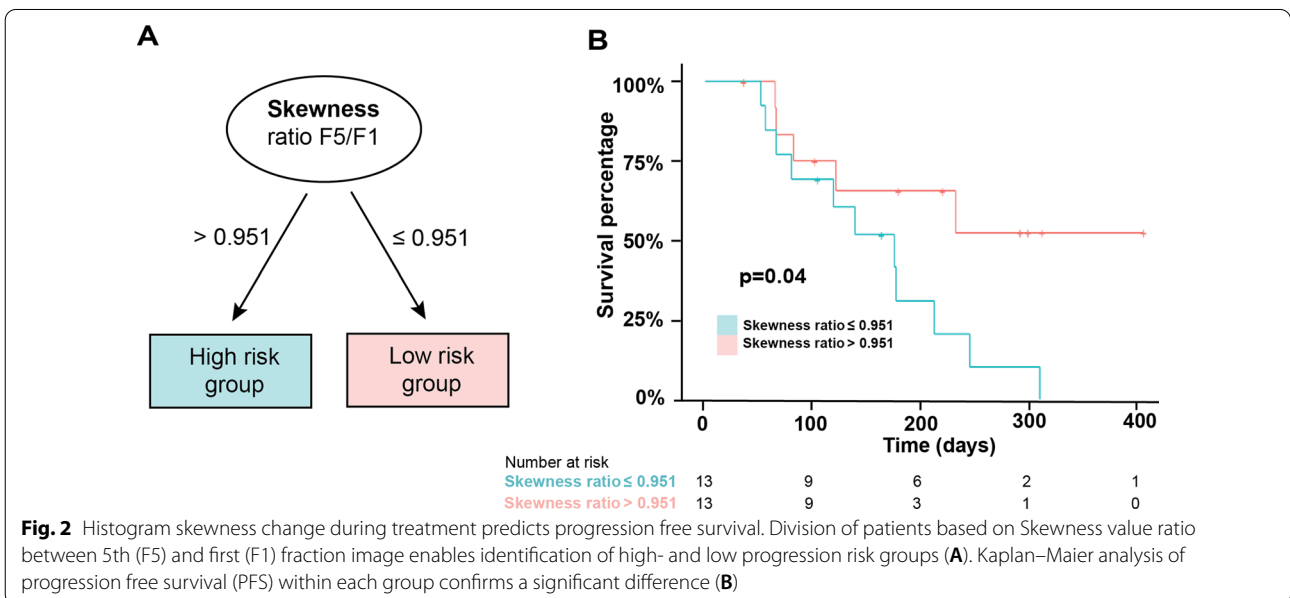
Image pre-processing is often required for quantitative analysis of MRI data to account for the lack of internal normalization. The signal intensities in the SIM and F1 scans, when no treatment had yet been administered and therefore no biological trends were expected, were compared to identify technical signal changes unrelated to radiation response. As shown in a representative patient (Fig. 1A, top row), a clear overall change in the image scaling without normalization was apparent. Following this observation, the median signal intensity ratio changes between F1 and SIM scans were compared in the GTV vs. the rest of the abdomen, to quantify the extent to which the intensity changes represented global, technical scaling drifts, as opposed to tumor-specific changes. A significant positive correlation (Pearson $r=0.50$, $p=0.009$, Fig. 1C) was observed across the patient cohort between the signal ratios in the two regions, strongly suggesting that non-normalized GTV signal intensity is overwhelmingly affected by the technical image scaling unrelated to biological treatment response, highlighting the importance of pre-processing. Following normalization to median kidney signal, the image intensity change in a representative patient was reduced (Fig. 1A, bottom row), and the global correlation to overall image scaling was no longer present (Fig. 1D). Normalization by division was chosen based on the linear shape of the relationship in Fig. 1C.

Notably, no significant association was observed between pre-treatment (simulation scan) MRgRT image features and the PFS ($p > 0.11$). The prognostic power of the image histogram changes for PFS was then investigated. A significant association between PFS and the F5/F1 ratio for histogram skewness was observed based on Cox proportional hazard model (Hazard Ratio 2.75 (1.36–5.56), $p=0.038$ post multiplicity correction). Other histogram features showed no association with disease progression (Table 1). The ROI volume, often strongly affecting feature quantification, showed



no correlation with histogram skewness ($p=0.43$), and no association with PFS ($p=0.40$). Importantly the treatment variables -dose delivered and the number of days between the first and last radiation fraction were also not associated with PFS ($p=0.15$ and $p=0.50$ respectively).

A conditional inference tree [20], a type of decision tree algorithm, was used to identify patient risk groups based on the Skewness change (Fig. 2), showing that the skewness of the F5/F1 ratio threshold can be used to differentiate patients with high risk of progression (Skewness Ratio > 0.95) from these with lower risk of progression



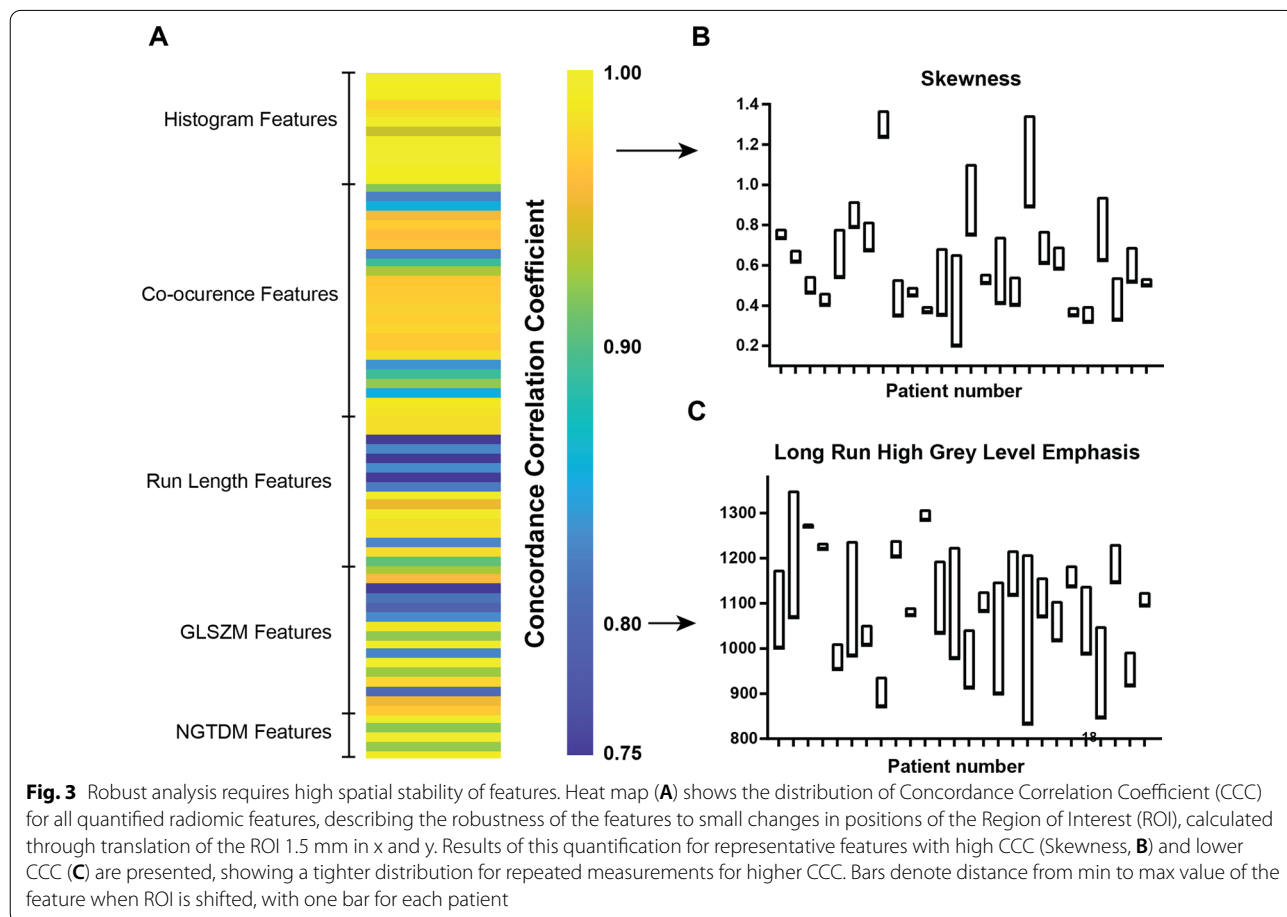
(Skewness Ratio ≤ 0.95 , Fig. 2A), with significantly different PFS between the groups ($p = 0.041$, see Fig. 2B for the Kaplan-Maier curves).

Association with PFS was also assessed for texture radiomic features. Contrary to the promising value of histogram quantification, despite over 60 features considered, borderline significant association ($p = 0.049$) was observed for one texture feature only (Cluster Shade), and only prior to multiplicity correction. The results are shown in Table 2. None of the histogram or texture features showed association with type of induction chemotherapy or resectability status.

Analysis of spatial robustness of MRgRT radiomics was performed for both histogram and texture features through quantification of feature changes following small changes in GTV boundary position. The Concordance Correlation Coefficient (CCC) of the feature values after ± 1.5 mm GTV erosion and dilation, simulating minor differences in ROI drawing, was calculated for each feature as a measure of stability and the results are shown in Fig. 3. High heterogeneity and clear patterns by feature type are observed in spatial robustness (Fig. 3A).

Good performance ($CCC > 0.935$) overall was measured for histogram features, a subset of co-occurrence matrix features related to inverse difference and a subset of Grey Level Size Zone Matrix (GLSZM) features related to non-uniformity. Importantly, skewness showed a good robustness compared to other features ($CCC = 0.972$, 62nd percentile). Serving as a visual example, the skewness values from shifted ROIs showed a tight distribution of each patient compared to the between-patient variability (Fig. 3B). On the other hand, poor spatial robustness, or high sensitivity of the feature to ROI shift as small as 1.5 mm, quantified in low CCC was noted for some features, e.g. grey level run emphasis features, as shown for High Grey Level Run Emphasis (Fig. 3C), for which the spread of the values for the perturbed ROIs is comparable to the dynamic range between patients.

Prior to treatment all but one tumor showed a mild positive (rightward) histogram skew (0.60 ± 0.06), with the group of patients more likely to progress (high-risk group) showing a further increase in right skewness during treatment ($F5/F1$ ratio = 1.52 ± 0.05), while the patients less likely to progress (low-risk group) showed



a decrease in skewness to a more normal distribution (F5/F1 ratio 0.60 ± 0.01). The observed changes during treatment for representative low and high-risk patients and the corresponding image histograms are shown in

Fig. 4, and while the histograms often shift considerably during treatment in both risk groups (Fig. 4A), these changes are difficult to discern visually in the images

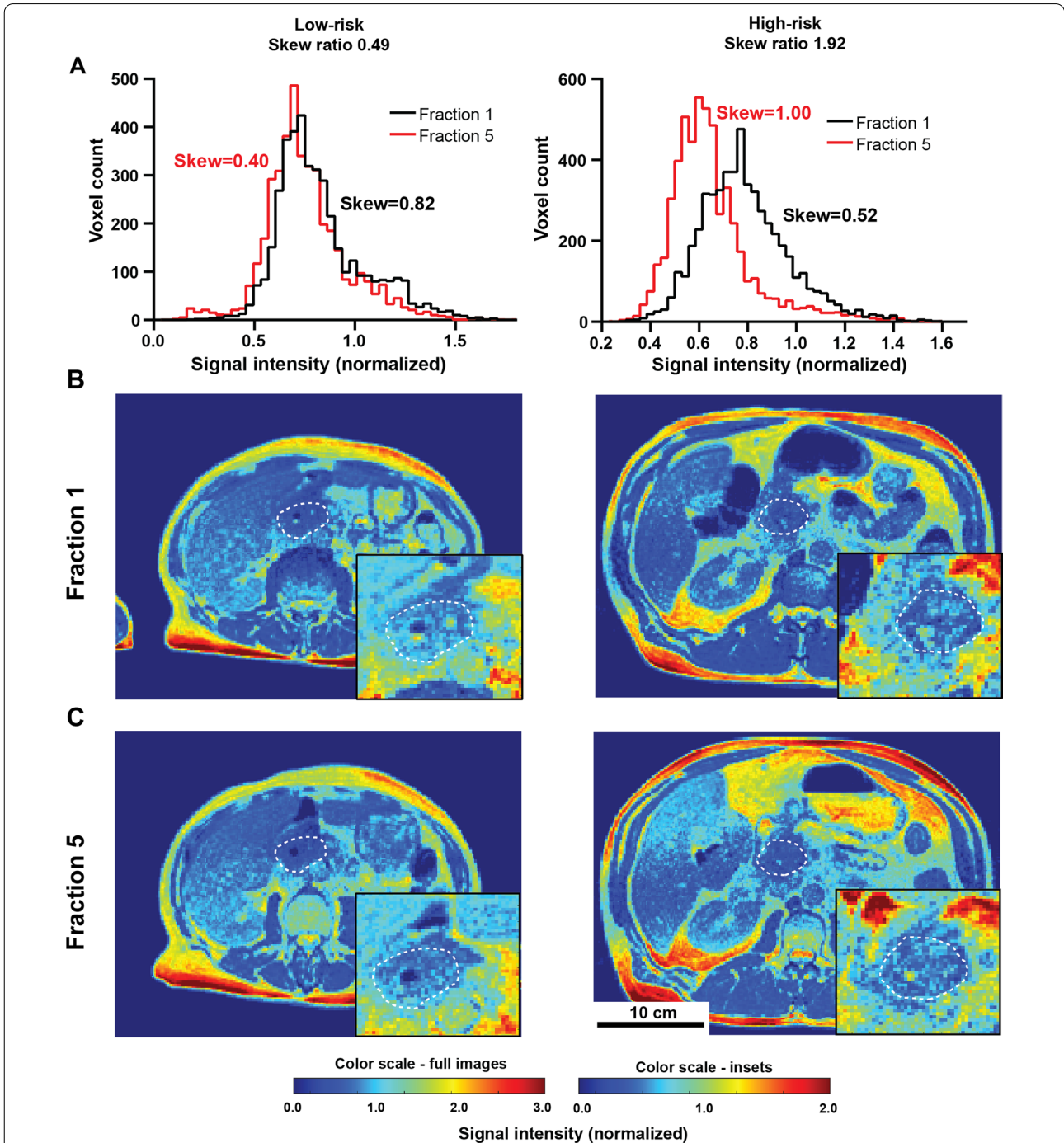


Fig. 4 Skewness changes during treatment are not clearly visible in the images. Histograms of the GTV signal intensity distributions at first (black) and last (red) fraction are shown in (A) for representative low risk (left) and high risk (right) patients. Axial slices through the body for these patients at first and last (5th) fraction are shown in (B) and (C) respectively, outlining the tumor cross-section in dotted white line. Magnified tumor area is shown in insets.

(Fig. 4B, C) highlighting the value of quantitative tools as presented in this paper.

Discussion

Magnetic Resonance Guided Radiation Therapy constitutes one of the most impactful developments in recent radiation oncology technologies. Beyond the direct improvement in dose delivery precision and motion management, the abundance of real time imaging data opens significant opportunities for automated radiomic image quantification [8]. Our previous work highlights the promise of histogram change quantification for prediction of radiation response in preclinical models of PDAC [21] in MRI. The results of this study reinforce this view, showing that subtle yet quantifiable changes in the tumor imaging characteristics during the course of SBRT may be strongly associated with disease progression in pancreatic cancer, paving the way for image-driven dynamic dose adaptation.

We hypothesized that the dynamic information available from the MRI scans at each radiation fraction may provide particularly valuable insight, quantifying the early effects of irradiation on the tumor. Rather than considering the static image features at fixed timepoints, the analysis was therefore focused on parameter ratios at last vs. first fraction delivered. Quantifying the change in histogram parameters, widely used in MR imaging for heterogeneity analysis [18], a strong association of histogram skewness change with progression free survival was observed. A measure of the asymmetry of the voxel intensity distribution, the skewness was found to increase during treatment for patients with high progression risk, while in non-progressing low-risk patients the skewness was more likely to decrease. While highly statistically significant and with clear mathematical meaning, the changes are not visually apparent, highlighting the value of computational radiomic analysis for identification of hidden imaging patterns.

Beyond demonstrating the relationship with outcome, the study is the first to develop the protocol for MRgRT image analytics. We show that linear image normalization not only reduces signal variability between scans but is required to remove technical global signal drift and identify the tumor-specific signal intensity changes. As part of previously untested technical validation of MRgRT radiomics, we discuss the spatial robustness of the quantified radiomic features. The anatomical characteristics of PDAC lesions, notoriously challenging to segment reliably, highlight the relevance of this analysis. While some feature groups showed high technical variability following small changes in segmentation, suggesting poor reproducibility, the work revealed multiple robust features, promising for further radiomic

studies. Conservative choice of small 1.5 mm ROI perturbation was designed to highlight the most unstable features to be avoided in future MRgRT radiomic analysis. Histogram features including the skewness were found to be highly spatially robust to these small changes. This is key for the clinical implementation of radiomic features into the clinical workflow. While this approach provides a robust automated framework for stability analysis, future work should also include direct measurements of inter- and intra-observer variability through repeated manual segmentation.

Progression free survival was chosen as the most appropriate and meaningful outcome metric, in line with the recent reports [5]. With a 60% event rate and follow-up as long as 13 months, the study was well-powered for identification of the observed progression patterns. Local control was not considered as the great majority of patients in this study (22/26) exhibited stable disease by RECIST, consistent with the low (10–20%) rate of local failure at 1 year in the literature.

Previous reports showed that radiomics may potentially be used to quantify image textures in MRgRT data, and relate them to outcome in pancreatic [12] and rectal cancers [10, 11] both in static and delta radiomic setting. Given the large number of features tested in small patient cohorts, as well as lack of image normalization, the results presented will require further validation. However, the rapidly increasing number of publications and conference presentations on the topic indicate significant interest in MRgRT radiomics. To minimize over-fitting in a small dataset, the analysis was limited to univariate signatures and focused firstly on histogram features. A larger study will be needed to verify the observed relationships, understand the link between radiomic features and treatment response, as well as to optimize the signatures through multivariate analysis. A higher-powered study may reveal further associations in the data not reported here, including relationships between pre-treatment imaging features and local control after irradiation, as reported in previous studies [12].

Given the increasing number of patients treated with this technology, a relatively simple pipeline required beyond standard of care to collect and analyze the data will enable quick accumulation of available data volume. This will soon allow for well-powered retrospective studies with 100 s of patients to be conducted. The uniformity of the acquisition settings between patients and imaging centers, especially on the 0.35T systems, will further accelerate the process, allowing for simpler multi-center collaborations, as already reported on a small scale [11]. Open access to the analytical pipeline developed in this study, including the necessary image

processing and quantification code, may contribute to further simplification of the process.

Histogram features have been discussed in numerous MRI studies as descriptors of tumor heterogeneity [22, 23]. In particular the skewness of several MRI parameters, representing the asymmetry of voxel value distribution, has been reported to correlate with prognosis and outcome [18], especially in brain cancer [24]. Skewness changes during therapy were found to predict response [25, 26], as reported in this study, for the first time in MRgRT. However, understanding of precise biological underpinnings of these confirmed relationships poses a significant challenge [27]. Compared to some more established quantitative MRI metrics such as k^{trans} or ADC the Balanced Steady State Free Precession sequence signal intensity, used as a core sequence in 0.35T MRgRT, has a less well-defined biological meaning. Further work, including analysis of additional correlates may be required to provide a definite explanation. Insight may also be provided through histological comparison between the imaging and pancreatic resection specimens as part of a clinical trial underway at our institution.

The data presented above suggests that delta radiomics of Magnetic Resonance guided Radiotherapy imaging data shows significant promise for prediction of patient radiotherapy response, based on early changes in tumor morphology during radiation treatment, quantified in MR scans using histogram analysis. With further research, the findings may shed more light on the role of intratumor heterogeneity in radiotherapy response potentially increasing the reliability of predicting which patients can proceed to R0 resection, which can dramatically improve survival.

Supplementary Information

The online version contains supplementary material available at <https://doi.org/10.1186/s13014-021-01957-5>.

Additional file 1. Supplementary Figure 1: Kidney Region of Interest. The regions of interest used for image normalization were drawn manually in three equally spaced slices of each scan. As shown in the example above, if the right kidney was present in slices 62-96, contours were drawn in slices representing $\frac{1}{4}$, $\frac{1}{2}$ and $\frac{3}{4}$ of the way through the kidney volume, and voxels from these 3 slices used for the kidney signal intensity quantification.

Acknowledgements

Not applicable.

Authors' contributions

RJG, SAR and MRT conceptualized the study, KL, JMF and SE collected, identified and curated the imaging data, MRT and KL processed the imaging data, EB and RFP collected and curated outcome data, MRT, IEN, EM and RJG designed the analysis, MRT performed the analysis and quantification, SAR and JMF provided clinical perspective for discussion, MRT and RJG wrote the draft. All authors read and approved the final manuscript.

Funding

This work was supported by NIH grants NIH 1U54CA193489, R01CA187532 and U01CA200464.

Availability of data and materials

All materials are available on request, and analysis code can be downloaded from a public repository https://github.com/mrtomasz91/MRgRT_PDAC.

Declarations

Ethics approval and consent to participate

The Institutional Review Board at the University of South Florida approved (IRB #20383) and waived the informed consent requirement for retrospective analysis in this study.

Consent for publication

Not applicable.

Competing interests

RJG has a competing interest as investor with research support from HealthMyne, Inc. (not used in current study). SHE received research support from Varian Medical Systems and ViewRay Inc and honoraria from Merck & Co. SAR reports consulting honoraria from Novocure, and research support and consulting honoraria from Viewray Inc. Other authors declare no potential conflicts of interest.

Author details

¹Cancer Physiology Department, H. Lee Moffitt Cancer Center and Research Institute, 12902 USF Magnolia Dr, Tampa, FL 33612, USA. ²Medical Physics Department, H. Lee Moffitt Cancer Center and Research Institute, Tampa, FL, USA. ³Radiation Oncology Department, H. Lee Moffitt Cancer Center and Research Institute, Tampa, FL, USA. ⁴Machine Learning Department, H. Lee Moffitt Cancer Center and Research Institute, Tampa, FL, USA. ⁵Present Address: Translation Imaging Department, Merck & Co, West Point, PA, USA.

Received: 13 August 2021 Accepted: 22 November 2021

Published online: 15 December 2021

References

- Siegel RL, Miller KD, Jemal A. Cancer statistics, 2019. *CA Cancer J Clin*. 2019;69(1):7–34.
- Iacobuzio-Donahue CA, Fu B, Yachida S, Luo M, Abe H, Henderson CM, et al. DPC4 gene status of the primary carcinoma correlates with patterns of failure in patients with pancreatic cancer. *J Clin Oncol*. 2009;27(11):1806–13.
- Krishnan S, Chadha AS, Suh Y, Chen HC, Rao A, Das P, et al. Focal radiation therapy dose escalation improves overall survival in locally advanced pancreatic cancer patients receiving induction chemotherapy and consolidative chemoradiation. *Int J Radiat Oncol Biol Phys*. 2016;94(4):755–65.
- Henke L, Kashani R, Robinson C, Curcuro A, DeWees T, Bradley J, et al. Phase I trial of stereotactic MR-guided online adaptive radiation therapy (SMART) for the treatment of oligometastatic or unresectable primary malignancies of the abdomen. *Radiother Oncol*. 2018;126(3):519–26.
- Chuong MD, Bryant J, Mittauer KE, Hall M, Kotecha R, Alvarez D, et al. Ablative 5-fraction stereotactic magnetic resonance-guided radiation therapy with on-table adaptive replanning and elective nodal irradiation for inoperable pancreas cancer. *Pract Radiat Oncol*. 2021;11(2):134–47.
- Blair AB, Krell RW, Ejaz A, Groot VP, Gemenetzis G, Padussis JC, et al. Proclivity to explore locally advanced pancreas cancer is not associated with surgeon volume. *J Gastrointest Surg*. 2021;25(10):2562–71.
- Gemenetzis G, Blair AB, Nagai M, Groot VP, Ding D, Javed AA, et al. Anatomic criteria determine resectability in locally advanced pancreatic cancer. *Ann Surg Oncol*. 2021.
- Gillies RJ, Kinahan PE, Hricak H. Radiomics: images are more than pictures, they are data. *Radiology*. 2016;278(2):563–77.
- Avanzo M, Wei L, Stancanella J, Vallières M, Rao A, Morin O, et al. Machine and deep learning methods for radiomics. *Med Phys*. 2020;47(5):185–202.

10. Boldrini L, Cusumano D, Chiloiro G, Casà C, Masciocchi C, Lenkowicz J, et al. Delta radiomics for rectal cancer response prediction with hybrid 0.35 T magnetic resonance-guided radiotherapy (MRgRT): a hypothesis-generating study for an innovative personalized medicine approach. *La Radiol Med*. 2019;124(2):145–53.
11. Cusumano D, Boldrini L, Yadav P, Casà C, Lee SL, Romano A, et al. Delta radiomics analysis for local control prediction in pancreatic cancer patients treated using magnetic resonance guided radiotherapy. *Diagnosics (Basel, Switzerland)*. 2021;11(1):72.
12. Simpson G, Spieler B, Dogan N, Portelance L, Mellon EA, Kwon D, et al. Predictive value of 0.35 T magnetic resonance imaging radiomic features in stereotactic ablative body radiotherapy of pancreatic cancer: a pilot study. *Med Phys*. 2020;47(8):3682–90.
13. Jethanandani A, Lin TA, Volpe S, Elhalawani H, Mohamed ASR, Yang P, et al. Exploring applications of radiomics in magnetic resonance imaging of head and neck cancer: a systematic review. *Front Oncol*. 2018;8:131.
14. Park JE, Park SY, Kim HJ, Kim HS. Reproducibility and generalizability in radiomics modeling: possible strategies in radiologic and statistical perspectives. *Korean J Radiol*. 2019;20(7):1124.
15. Zwanenburg A, Leger S, Vallières M, Löck S. Image biomarker standardisation initiative. 2016.
16. Bieri O, Scheffler K. Fundamentals of balanced steady state free precession MRI. *J Magn Reson Imaging*. 2013;38(1):2–11.
17. Vallières M, Freeman CR, Skamene SR, El Naqa I. A radiomics model from joint FDG-PET and MRI texture features for the prediction of lung metastases in soft-tissue sarcomas of the extremities. *Phys Med Biol*. 2015;60(14):5471–96.
18. Just N. Improving tumour heterogeneity MRI assessment with histograms. *Br J Cancer*. 2014;111(12):2205–13.
19. Lin LI. A concordance correlation coefficient to evaluate reproducibility. *Biometrics*. 1989;45(1):255–268.
20. Sardá-Espinosa A, Subbiah S, Bartz-Beielstein T. Conditional inference trees for knowledge extraction from motor health condition data. *Eng Appl Artif Intell*. 2017;62:26–37.
21. Tomaszewski MR, Dominguez-Viqueira W, Ortiz A, Shi Y, Costello JR, Enderling H, et al. Heterogeneity analysis of MRI T2 maps for measurement of early tumor response to radiotherapy. *NMR Biomed*. 2021;34(3):e4414.
22. Alic L, Niessen WJ, Veenland JF. Quantification of heterogeneity as a biomarker in tumor imaging: a systematic review. *PLoS ONE*. 2014;9(10):e110300.
23. O'Connor JPB, Rose CJ, Waterton JC, Carano RAD, Parker GJM, Jackson A. Imaging intratumor heterogeneity: role in therapy response, resistance, and clinical outcome. *Clin Cancer Res*. 2015;21:249–57.
24. Tozer DJ, Jäger HR, Danchaivijitr N, Benton CE, Tofts PS, Rees JH, et al. Apparent diffusion coefficient histograms may predict low-grade glioma subtype. *NMR Biomed*. 2007;20(1):49–57.
25. Nowosielski M, Recheis W, Goebel G, Güler O, Tinkhauser G, Kosttron H, et al. ADC histograms predict response to anti-angiogenic therapy in patients with recurrent high-grade glioma. *Neuroradiology*. 2011;53(4):291–302.
26. Baek HJ, Kim HS, Kim N, Choi YJ, Kim YJ. Percent change of perfusion skewness and kurtosis: a potential imaging biomarker for early treatment response in patients with newly diagnosed glioblastomas. *Radiology*. 2012;264(3):834–43.
27. Tomaszewski MR, Gillies RJ. The biological meaning of radiomic features. *Radiology*. 2021;299(2):E256.

Publisher's Note

Springer Nature remains neutral with regard to jurisdictional claims in published maps and institutional affiliations.

Ready to submit your research? Choose BMC and benefit from:

- fast, convenient online submission
- thorough peer review by experienced researchers in your field
- rapid publication on acceptance
- support for research data, including large and complex data types
- gold Open Access which fosters wider collaboration and increased citations
- maximum visibility for your research: over 100M website views per year

At BMC, research is always in progress.

Learn more biomedcentral.com/submissions

